New Journal of Physics
The open-access journal for physics

Structure and magnetism of cobalt-doped ZnO thin films

M Ivill[1], S J Pearton[1], S Rawal[1], L Leu[1], P Sadik[1], R Das[2], A F Hebard[2], M Chisholm[3], J D Budai[3] and D P Norton[1,4]

[1] Materials Science and Engineering, University of Florida, Gainesville, FL 32611, USA
[2] Department of Physics, University of Florida, Gainesville, FL 32611, USA
[3] Oak Ridge National Laboratory, Oak Ridge, TN 37831, USA
E-mail: dnort@mse.ufl.edu

New Journal of Physics **10** (2008) 065002 (21pp)
Received 7 February 2008
Published 6 June 2008
Online at http://www.njp.org/
doi:10.1088/1367-2630/10/6/065002

Abstract. The structure and magnetic properties of Co-doped ZnO films are discussed in relation to cobalt doping levels and growth conditions. Films were deposited by pulsed-laser deposition (PLD) from ZnO targets containing cobalt concentrations from 0 to 30 at.%. The structure of the films is examined by x-ray diffraction (XRD) and transmission electron microscopy (TEM), and optical absorption is used to infer the substitution of cobalt inside the ZnO lattice. Magnetic properties are characterized by superconducting quantum interference device (SQUID) magnetometry. Films doped with cobalt concentrations of a few per cent appear to be composed of two magnetic components: a paramagnetic component and a low-field ferromagnetic component. Films doped with 30% cobalt show a larger FM signature at room temperature with clear hysteretic shape, but films grown at low pressure are plagued by the precipitation of metallic cobalt nanoparticles within the lattice which can be easily detected by XRD. These particles are well oriented with the ZnO crystal structure. By increasing the base pressure of the vacuum chamber to pressures above 1×10^{-5} Torr, metallic cobalt precipitates are undetectable in XRD scans, whereas the films still show an FM signature of $\sim 0.08\,\mu_B$/Co. Depositions in the presence of oxygen background gas at 0.02 mTorr decreases the magnetization. The decreased magnetization with oxygen suggests that the activation of

[4] Author to whom any correspondence should be addressed.

ferromagnetism depends on defects, such as oxygen vacancies, created during growth. Optical absorption measurements show a sequential increase in the Co^{+2} absorption peaks in these films, along with an almost linearly increasing bandgap with cobalt concentration suggesting a large solubility of cobalt in ZnO. Bright-field TEM imaging and electron diffraction do not show signs of precipitation; however, dark-field imaging shows circular areas of varying contrast which could be associated with cobalt precipitation. Therefore, the possibility that ferromagnetism results from secondary phases cannot be ruled out.

Contents

1. Introduction

Transition metal doped ZnO is a promising candidate material for the field of spin-electronics. Spin-electronics (or spintronics) is based on concepts that utilize the quantum mechanical spin properties of carriers in addition to the carrier charge in realizing electronic functionality [1, 2]. Carrier spins are used to transport, store and process information in novel ways, providing both enhanced performance and new functionalities in traditional microelectronic devices. Dilute magnetic semiconductors (DMS)—semiconductors doped with a few per cent of magnetic atoms—are being actively investigated in the development of spintronic devices. The magnetic properties of a DMS are intimately coupled to the carrier concentration and carrier type within the material through the s–d and p–d exchange integrals. This is beneficial in that it allows external control over the magnetic properties by electronically or optically manipulating the carriers in the DMS. For example, this type of external control has been demonstrated in (In,Mn)As using an electric field-gated structure [3]. While there has been much work on the III–V DMS materials, notably (In,Mn)As and (Ga,Mn)As, their ferromagnetic Curie temperatures (T_c) (90 K for (In,Mn)As [4] and 172 K for (Ga,Mn)As [5]) are too low for practical applications. The realization of practical commercial or mobile devices will require the development of semiconductors that can retain their FM properties above room temperature. As a result, significant research effort has been focused on developing alternative DMS materials with higher Curie temperatures [6, 7].

ZnO is an interesting direct wide bandgap semiconductor that is being explored for numerous applications [8]. The motivation for studying semiconducting oxides [9, 10], particularly ZnO, for spintronics was stimulated by the work of Dietl *et al* [11]. Dietl predicted

that heavily p-type, Mn-doped ZnO and GaN would have a Curie temperature above room temperature. The theory is based on an indirect exchange mechanism where the ferromagnetism between magnetic dopants is mediated by holes in the valence band. P-type material was predicted to result in high T_c primarily because both the exchange integral parameter and the density of states are higher in the valence band than the conduction band. Dietl's theory has proven useful in understanding the experimental results for GaMnAs. However, it does not appear to be consistent with the experimental results for transition metal doped wide bandgap semiconductors, such as ZnO and GaN. This stems from several reasons, including the difficulty in experimentally preparing p-type ZnO material and the many observations of ferromagnetism in n-type ZnO DMS. Nevertheless, Dietl's original theory has led to multiple experimental and computational studies of transition metal doping in ZnO and GaN [12]–[23].

Coey *et al* [24] have proposed another model for ferromagnetism in DMS materials based on a spin-split donor impurity band. This model provides a mechanism where ferromagnetism is influenced by defect states in the material. In the model, donor defects (which could arise from either oxygen vacancies or zinc interstitials in the case of ZnO) overlap at large concentrations to form an impurity band. The impurity band can interact with local magnetic moments through the formation of bound magnetic polarons (BMP). Within each BMP, the bound carrier interacts with the magnetic dopants inside its radius and can align the spins of the magnetic dopants parallel to one another. Ferromagnetism is achieved when the BMPs start to overlap to form a continuous chain throughout the material, thus percolating ferromagnetism in the DMS. However, Coey showed that in this model to achieve a high T_c a fraction of the polaronic charge must delocalize (or hybridize) onto each magnetic dopant. In a band scheme, this occurs when the impurity band overlaps with unoccupied d-levels of the magnetic dopant.

Within a similar framework to Coey's model, Kittilstved *et al* [25] have performed detailed spectroscopic experiments on cobalt-doped ZnO. Their results show that the singly ionized Co^{+} state lies close to the conduction band, similar in energy to a shallow donor state. Since the energies are similar, charge transfer (CT) can occur between the cobalt atoms and the donor impurities, thus leading to the hybridization necessary for ferromagnetism. Kittilstved *et al* have also shown that this leads to an inherent polarity difference for ferromagnetism in cobalt- and manganese-doped ZnO. Whereas ferromagnetism in cobalt-doped ZnO is closely tied to the presence of shallow donors, manganese-doped ZnO is closely tied to the presence of shallow acceptors. The difference lies in the location of the singly ionized Mn^{+3} state, which sits close to the valence band in ZnO. Consistent results have been reported for carrier-doped ZnO:Mn films [26, 27].

One of the early works on cobalt-doped ZnO by Ueda *et al* [28] showed promising results. They found the material to be FM above 280 K with 5–25% Co and 1% Al (added as an n-type dopant) without the addition of secondary phases [28]. Since then, additional experimental and computational studies have investigated the properties and origins of ferromagnetism in cobalt-doped ZnO. Many results have been reported with contradicting results between research groups. Some groups observe room temperature ferromagnetism in the absence of secondary phases or cobalt clusters [29]–[31]. However, others report no ferromagnetism at room temperature [32, 33], or that the observed ferromagnetism originates from metallic cobalt clusters [34, 35]. X-ray magnetic circular dichroism (XMCD) measurements have shown that dissolved cobalt atoms produce purely paramagnetic behavior, but that a ferromagnetic component is present which is possibly from defects created in the material [18, 36].

Other studies have also elucidated the importance of carriers and defects in mediating ferromagnetism in ZnO. Tuan *et al* [37] found that weak ferromagnetism in Co-doped ZnO films can be activated by post-growth vacuum annealing, changing the films from insulating to semiconducting behavior. The specific role of Zn interstitials has also been studied. Zn interstitials are believed to form a shallow donor state in ZnO. Reversible on/off ferromagnetic ordering at room temperature in chemically synthesized Co-doped ZnO films was achieved by the controlled incorporation and removal of Zn interstitials [38]. Zn interstitials were introduced by annealing in the presence of Zn vapor, and subsequently removed by annealing in oxygen. The interstitials were believed to activate ferromagnetism by introducing electrons, which were removed by oxidation. Khare *et al* [39] have also investigated the role of Zn interstitials. They also found that the magnetization in Co-doped ZnO is enhanced by introducing Zn interstitials into the lattice during annealing, but that the magnetization did not depend on carrier concentration. Their results also indicated that oxygen vacancies were not responsible for changes in magnetization. However, recent theoretical modeling does suggest that Co^{+2}–oxygen vacancy pairs are capable of promoting long-range FM coupling in the presence of n-type doping [40]. It seems, therefore, the recent literature suggests that ferromagnetism in Co-doped ZnO is highly dependant on intrinsic defects in the material. These defects may rely on the presence of the transition metal dopants by the formation of complexes that mediate FM ordering, or defects alone may be enough to cause ferromagnetism, such as that reported for undoped HfO_2 [41].

In this work, the structure and magnetic behavior of cobalt-doped ZnO thin films are examined. Cobalt concentration is varied over a wide range, with x-ray diffraction (XRD) and transmission electron microscopy (TEM) used to examine phase segregation. UV–Vis optical absorption measurements confirm the substitution of cobalt on Zn lattice sites and are used to infer the solubility of cobalt at large concentrations. Superconducting quantum interference device (SQUID) magnetometry is employed to measure the magnetic properties of the films. Films doped with 30% Co show the largest magnetization per cobalt atom. The magnetization and hysteresis drastically decreases for 30% Co-doped films deposited in oxygen, suggesting that the ferromagnetism depends on oxygen vacancy related defects created during the growth.

2. Experiment

Cobalt-doped ZnO epitaxial films were deposited via pulsed laser deposition (PLD) [42] onto *c*-plane oriented sapphire substrates. The ablation targets were prepared through the solid-state reaction of mixed oxide powders. Appropriate amounts of ZnO (Alfa Aesar, Puratronic®, 99.9995%) and Co_3O_4 (Alfa Aesar, Puratronic®, 99.9985%) powders were ground and mixed in methanol, dried in air, pressed into pellets and sintered at 1000 °C for 12 h in air. The targets were mixed to give proportions of $Zn_{1-x}Co_xO$ with $x = 0.00$, 0.02, 0.05, 0.10, 0.15 and 0.30. A KrF excimer laser (248 nm wavelength) was used for target ablation using a repetition rate of 1 Hz and a laser energy density of 1–3 J cm^{-2}. The target-to-substrate distance was 5.5 cm. A temperature range of 400–600 °C and oxygen pressures up to 0.02 mTorr were used in the experiments. The PLD system is evacuated using a turbomolecular pump to a base pressure of $\sim 7.0 \times 10^{-6}$ Torr. Film thicknesses were 150–250 nm as measured by mechanical profilometry.

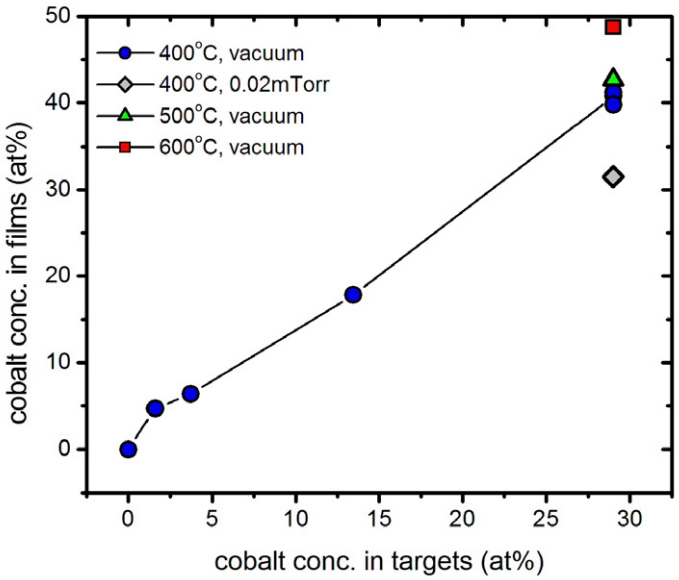

Figure 1. EDS results for a selected number of ZnO:Co films grown under different conditions. The data show the cobalt concentration in the films as compared to the cobalt concentration in the target.

3. Results and discussion

Energy dispersive spectroscopy (EDS) was used to measure the percentage of cobalt in the films. Figure 1 shows the cobalt concentration in the film as a function of target composition for films deposited under different conditions. The cobalt concentration is greater in the films than the prepared targets. Similar results of transition metal enrichment in doped ZnO films grown by PLD have been reported [30, 43, 44]. Dorneles *et al* [43] suggest that this difference in stoichiometry is caused by preferential sputtering of Zn as compared to the transition metal dopant. Also notice, for films doped with nominally 30% Co, the cobalt concentration is slightly higher with increased substrate temperature and slightly lower with a small addition of oxygen background gas.

3.1. Films grown in low-base pressure

Crystal structure and phase analysis were characterized using XRD in Bragg–Brentano geometry. A step size of 0.02° and time-per-step of 1.25 s were used for each scan. Figure 2 shows the θ–2θ XRD patterns for a series of films grown at 400 °C in vacuum (base pressure $\sim 7 \times 10^{-6}$ Torr) with varying cobalt concentration. The primary peaks correspond to the wurtzite ZnO (002) indicating good texture with the *c*-plane of the sapphire substrate. There is a small peak noticeable in some of the Co-doped films around $2\theta = 44.4°$. This peak is consistently recorded at 15 and 30% cobalt and occasionally seen in films with lower cobalt concentrations, such as the film with 5% Co in figure 2. The peak intensity is low (only a few hundred counts above background) and does not correspond to any ZnO or substrate peaks. Both the small intensity and 2θ position make identification of the peak difficult using XRD as there are several cobalt containing phases with similar 2θ values of around 44.4°, including

Table 1. Possible cobalt-induced secondary phases.

Phase	Structure	2θ (degrees)	Coupling	T^* (K)
Co	Cubic (111)	44.216	FM	$T_c = 1373$
	Hex (0002)	44.762		
CoO	Cubic (200)	42.401	AFM	$T_n = 291$
Co_3O_4	Spinel (400)	44.808	AFM	$T_n = 30$
$ZnCo_2O_4$	Spinel (400)	44.738	AFM (n-type)	N/A [48]
			FM (p-type)	
$CoAl_2O_4$	Spinel (400)	44.692	AFM	$T_n < 40$

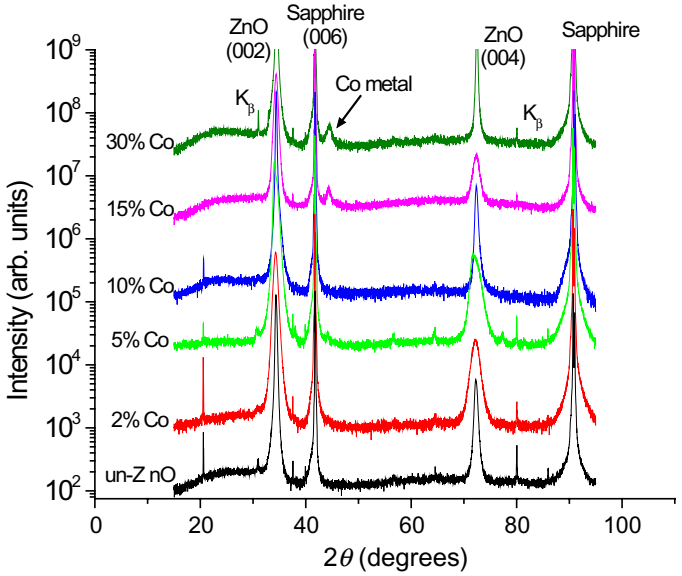

Figure 2. XRD scans for a series of ZnO : Co films grown in vacuum at 400 °C. The films are predominantly *c*-axis oriented ZnO. At high cobalt concentrations, cobalt metal precipitation appears (corresponding to the peak near $2\theta = 44.4°$).

the spinel family of cobalt oxides and cobalt metal [45]. A longer scan (step size = 0.005° and time/step = 5.0 s) around this peak, performed on the film with 30% Co, shows one broad Gaussian peak and does not show signs of asymmetry or overlapping peaks. Determination of the phase responsible for the peak is critical since the presence of ferromagnetic cobalt metal could contribute to the magnetic signature of the films. The cubic and spinel cobalt oxides are antiferromagnetic, though some papers report that small nanocluster powders of cobalt oxides are ferromagnetic due to uncompensated surface spins [46, 47]. Table 1 is a list of the possible phases with their 2θ diffraction values and magnetic character.

There is an asymmetric broadening on the high-angle side of the ZnO (002) and (004) diffraction peaks with the addition of cobalt. The asymmetry is not necessarily a function of Co concentration, as can be seen from the ZnO (004) broadening in figure 2. A similar peak broadening has been reported for $Zn_{0.75}Co_{0.25}O$ films grown on SiO_2/Si substrates [49]. The asymmetry may represent a stress gradient along the *c*-axis of the ZnO [50] or imperfect texturing of crystalline grains [49].

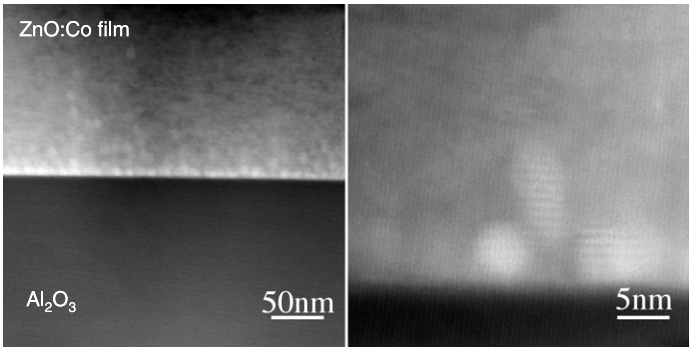

Figure 3. TEM micrographs of a sample doped with 30 at.% Co. This film shows the presence of metallic cobalt in the XRD scan. The precipitation appears mostly at the substrate/film interface in the form of ∼5 nm particles.

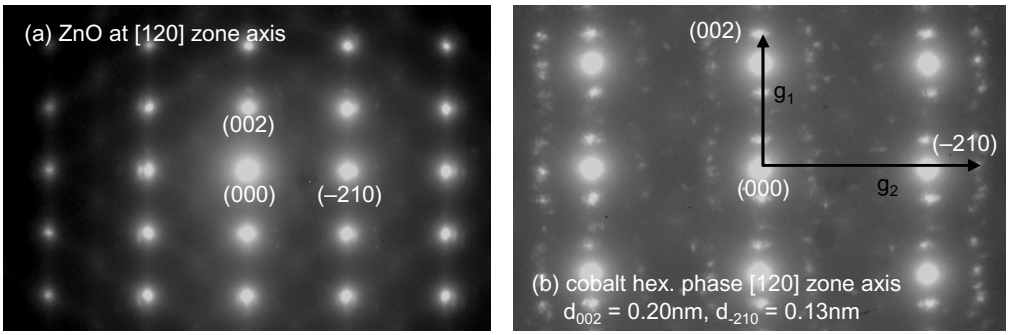

Figure 4. Selected area TEM diffraction patterns of a ZnO film doped with 30 at.% Co grown at 400 °C in vacuum. (a) Wurtzite ZnO along [120] zone axis and (b) ZnO + nano-particles along [120] zone axis with $d_{002} = 0.20$ nm and $d_{-210} = 0.13$ nm, which is consistent with metallic cobalt.

High resolution XRD and TEM were used to characterize the secondary phase observed in the powder XRD scans. Cross-sectional TEM was used to more precisely delineate the nature and location of the extra phase as shown in figure 3. Most of the precipitation occurs near the film/substrate interface in the form of small (∼5 nm) particulates. However, for most of the film, the cobalt dopant appears to reside in the ZnO lattice without precipitation. TEM diffraction patterns of the film and nano-precipitates are shown in figure 4. The particles appear to be oriented with the lattice and have d-spacings of $d_{002} = 0.20$ nm and $d_{-210} = 0.13$ nm. This is consistent with metallic cobalt which can exist in either a hexagonal or face-centered cubic structure. Oriented cobalt nanoparticles have also been observed in ion-implanted cobalt-doped ZnO [51].

At higher growth temperatures, cobalt precipitates out of the lattice as CoO. Figure 5(a) shows XRD scans for films deposited at 500 and 600 °C in vacuum. At 500 °C the CoO phase begins to form along with the cobalt metal. At 600 °C the cobalt metal phase disappears and the CoO phase becomes prominent. Thermodynamically, CoO is the most stable phase at these temperatures and pressures. This can be seen from the thermodynamic predominance diagram

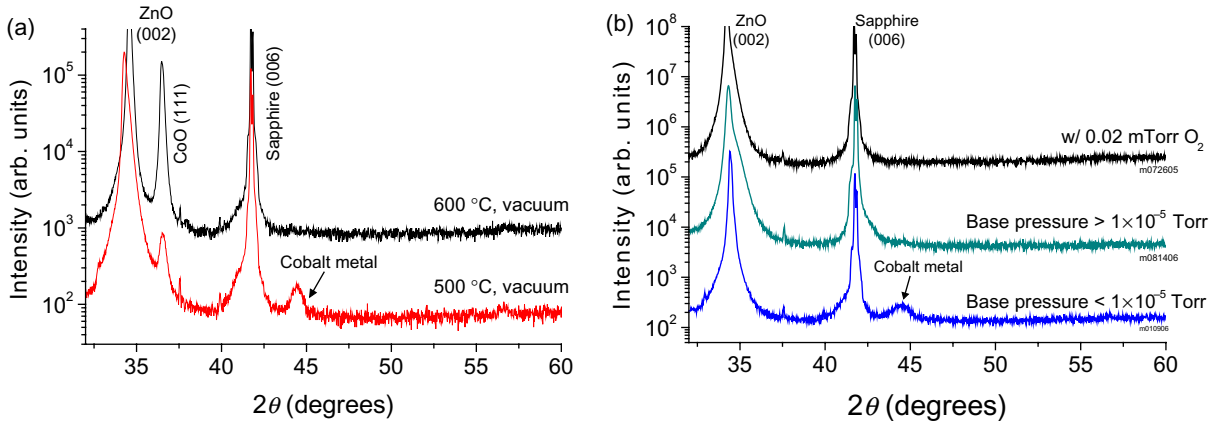

Figure 5. XRD scans for ZnO films doped with 30 at.% Co. (a) Films deposited at 500 and 600 °C in vacuum. (b) Films deposited at 400 °C under different pressure conditions.

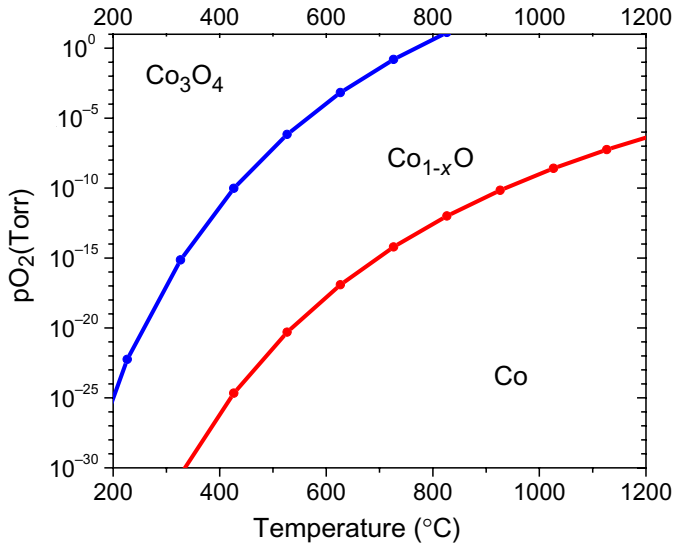

Figure 6. Thermodynamic predominance diagram for cobalt and cobalt oxides. Calculated using thermochemical values in [52].

for cobalt oxide given in figure 6. Interestingly, the formation of Co_3O_4 is expected at lower growth temperatures and not the metallic cobalt phase determined from TEM. This suggests that the cobalt metal phase is thermodynamically metastable, but gains some structural stability from the ZnO lattice. This is consistent with the well-oriented particles observed in TEM.

3.2. Films grown in higher base pressure

Films doped with 30% Co were grown under different pressure conditions in an attempt to suppress the formation of the metallic cobalt precipitates. By modifying the growth conditions, the secondary cobalt phase could be reduced. Figure 5(b) shows XRD scans for samples grown

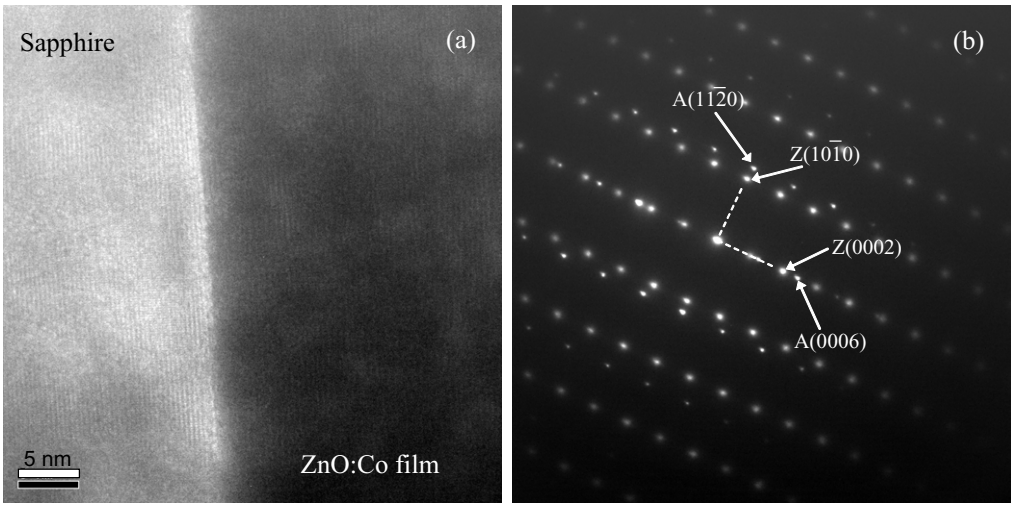

Figure 7. (a) Bright-field TEM image of the sapphire and ZnO:30% Co film interface. (b) Selected-area diffraction pattern of the interface region. A and Z denote the sapphire and ZnO:Co diffraction spots, respectively.

at 400 °C under different pressure conditions. The cobalt phase forms at low base pressures. By depositing in higher residual base pressures ($>10^{-5}$ Torr) or adding a small amount of oxygen, the Co phase disappears from the XRD scans. It should be noted that the process is not fully reproducible. The cobalt phase is still present by XRD for some depositions but is suppressed in roughly 80–90% of the samples grown in higher base pressures. It is assumed that the pressure at vacuum is composed mostly of water vapor, hydrogen and some molecular oxygen.

Since XRD alone may not be a sufficiently sensitive method for identifying precipitate formation, further analysis was carried out using TEM. Figure 7(a) shows a bright-field TEM image of the heavily doped ZnO:Co film and sapphire substrate. There does not appear to be any secondary-phase precipitation in the film. Additionally, in figure 7(b), the selected-area diffraction of the film and substrate reveals only the diffraction patterns of the sapphire substrate and ZnO lattice aligned with one another. However, viewing the film via dark-field imaging, the areas of brighter contrast near the substrate interface become apparent which could be associated with precipitate formation (figure 8). EDS analysis on dark and bright areas give roughly equal cobalt concentrations.

X-ray photoelectron spectroscopy (XPS) was also utilized to characterize the film. A Perkin-Elmer PHI 5100 XPS system was used to collect data using an Al K_α x-ray source. Figure 9 shows an XPS spectrum of the Co 2p binding energies. The data are given after sputtering the film for 5 min with 4 keV Ar^+ ions at an angle of 45° relative to the film surface. Both Zn and Co 2p peak intensities for this particular sample were low before sputtering due to surface contamination. Before sputtering, the binding energy of the adventitious carbon 1s peak was located around 287.5 eV. However, after sputtering, the carbon 1s peak disappeared and could not be used as an internal reference to correct for charging. Instead, the data were shifted negative 5 eV in order to align the O 1s peak to 530.2 eV, which is a typical binding energy reported for the O 1s peak in ZnO [53]. The $2p_{3/2}$ peak located at 780.5 eV is due to the Co^{+2} oxidation state. The shake-up structure (labeled 's' in the figure) and the energy separation ($\Delta = 15.6$ eV) between the $2p_{3/2}$ and $2p_{1/2}$ peaks are consistent with divalent cobalt [54]. Since

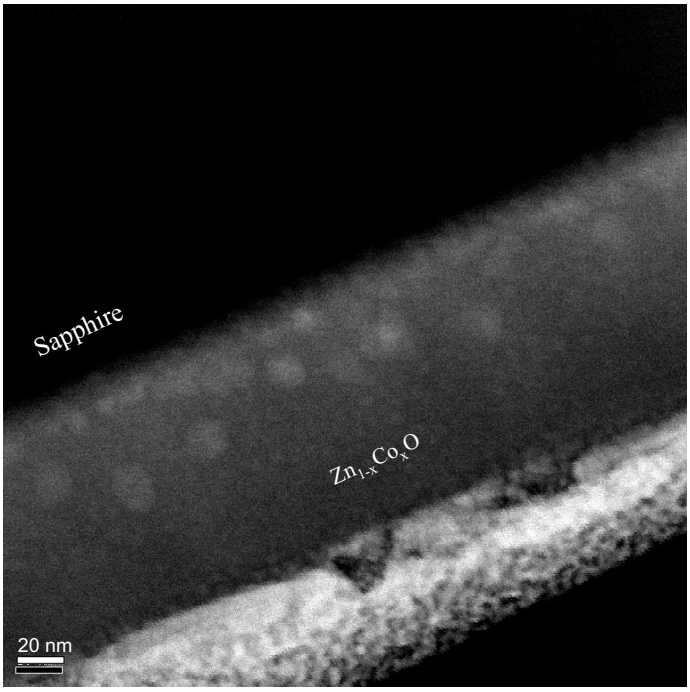

Figure 8. Dark-field TEM image of the ZnO:30% Co film showing areas of brighter contrast that could be related to precipitate formation.

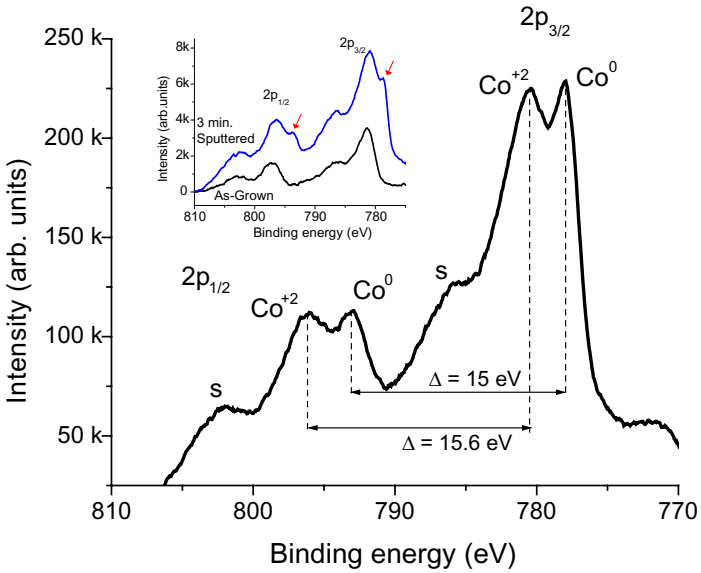

Figure 9. Co 2p XPS spectrum of ZnO:30% Co film after sputtering for 5 min. Peaks are assigned as metallic cobalt (Co^0), divalent cobalt (Co^{+2}), and Co^{+2} shake-up satellites (labeled 's'). The inset shows XPS spectra for a different ZnO:30% Co film as-grown and after 3 min sputtering. The arrows indicate the appearance of cobalt metal peaks after sputtering.

XRD excludes the possibility of cobalt oxide phases in the film, the data indicate a substantial portion of the cobalt atoms are Co^{+2} substituting on the Zn^{+2} lattice sites in ZnO. The lower binding energy $2p_{3/2}$ peak at 778 eV with $\Delta = 15$ eV is attributed to cobalt metal (Co^0) [54]. This likely indicates the inclusion of cobalt metal species in the film. However, sputter reduction of cobaltous ions at the film surface from argon bombardment is also a possibility [55]. Some of the ZnO films with nominally 30% Co have shown the appearance of cobalt metal peaks after Ar^+ sputtering in the XPS. The inset of figure 9 shows the Co 2p spectrum for a ZnO:30% Co film before and after sputtering for 3 min. The as-grown film shows only those peaks associated with the Co^{+2} oxidation state. However, after sputtering, Co^0 peaks appear showing the presence of metallic cobalt. There are two possible conclusions for the appearance of metallic cobalt in the XPS data. The first is that the film contains metallic cobalt clustering beneath the surface of the film. The surface sensitivity of XPS depends on the electron escape depth of the material; for ZnO the escape depth is estimated to be 3–10 nm [56]. The initial absence of the Co^0 peaks could be because the precipitates reside slightly further from the surface, or the metallic cobalt is oxidized at the film surface resulting in a higher oxidation state only in the surface region. The second possibility is that the cobalt is in the +2 oxidation state and is reduced at the film surface from Ar^+ sputtering. Since large amounts of metastable Co^{+2} are present in the film, they may be susceptible to reduction during sputtering in vacuum. We have not seen any other results in the recent literature describing sputter reduction of Co-doped ZnO films supporting this conclusion. More detailed characterization and XPS measurements as a function of sputtering time would be needed to clarify the data.

3.3. Optical properties

The four-fold coordinated ionic radii of Co^{+2} (0.058 nm) and Zn^{+2} (0.06 nm) are very similar and result in a large solubility of Co^{+2} in the ZnO lattice [57]. Many groups have confirmed that Co atomically substitutes on Zn sites using a variety of methods, including EXAFS [58, 59], XPS [37], [60]–[62], MCD [18, 37, 57, 59], XAS [36, 59, 63], ESR [64], XANES [65] and optical absorption [30, 37, 57, 66, 67]. Evidence for Co substitution in the ZnO lattice for our films can be inferred from optical absorption measurements. Figure 10 shows the optical transmission for Co-doped ZnO films that do not show cobalt precipitation by XRD. An undoped ZnO film is included as reference. Three absorption peaks are apparent in the doped films. These peaks are characteristic d–d transition levels attributed to Co^{+2} occupying tetrahedral lattice positions, and indicate that cobalt is substituting as Co^{+2} on Zn lattice sites in the films; these peaks are reported in multiple publications on $Zn_{1-x}Co_xO$ films as mentioned above. Specifically, the peaks located at energies of 1.9 eV (651 nm), 2.0 eV (608 nm) and 2.2 eV (564 nm) correspond to the $^4A_2 \rightarrow {}^2E(G)$, $^4A_2 \rightarrow {}^4T_1(P)$ and $^4A_2 \rightarrow {}^2A_1(G)$, respectively [68]. It is difficult to quantify the absorbance due to the Co^{+2} d–d transitions since the overall value of the transmittance for each film is different. For example, there exist crossovers in the data between 15 and 30%, and also between 10 and 2%. The crossovers may be from the difference in film thickness, which is measured to be ∼30% between the thinnest and thickest films. To examine the absorption due to the characteristic Co^{+2} transitions, the absorption coefficient versus cobalt concentration was plotted and the area underneath the absorption wells between 1.7 and 2.4 eV (the relevant range for the characteristic Co^{+2} transitions) was calculated. The absorption coefficient was used since it is normalized by the film thickness. The calculated area as a function of cobalt is presented in figure 11. The absorptions from the Co^{+2} ions increase

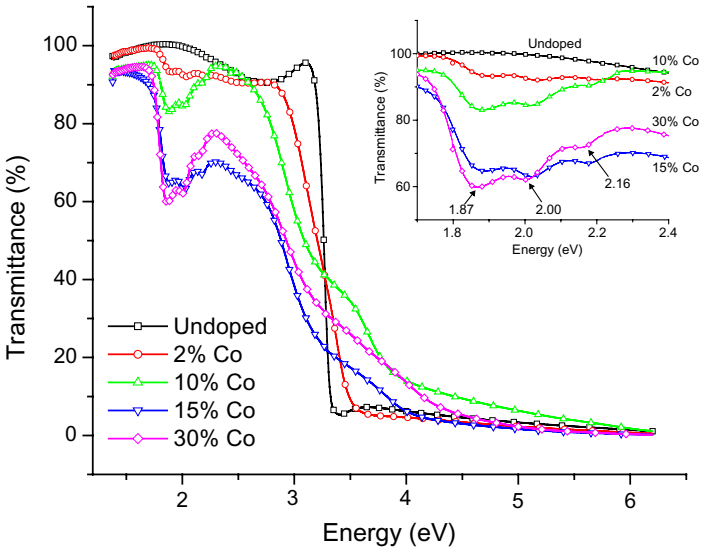

Figure 10. UV–Vis transmission of Co-doped ZnO films deposited in vacuum at 400 °C. The inset shows a close-up view of the absorption levels corresponding to Co^{+2} in wurtzite ZnO.

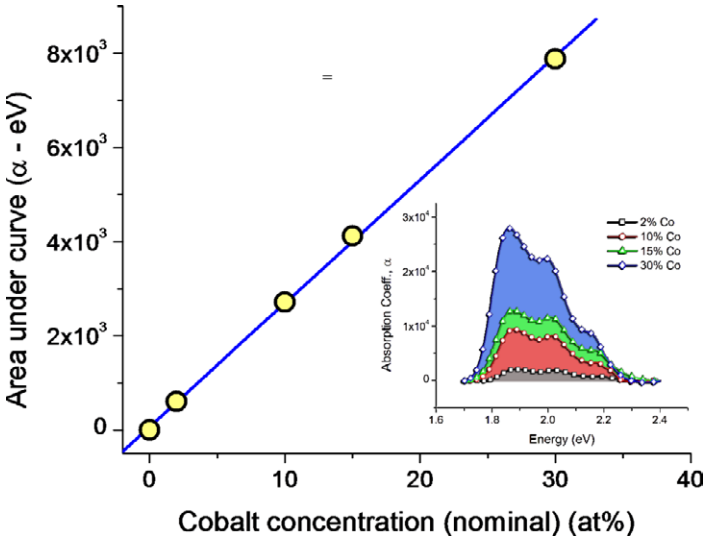

Figure 11. The calculated area underneath the characteristic absorption wells plotted as a function of cobalt concentration. Inset: the absorption coefficient (baseline subtracted) between 1.7 and 2.4 eV measured from the ZnO:Co films.

with the Co concentration suggesting that most of the cobalt is dissolved in the lattice. The inset of figure 11 shows the baseline subtracted absorption wells between 1.7 and 2.4 eV for the film.

The bandgap of the alloys was determined using Tauc plots. The absorption coefficient, α, for direct interband transitions is given by the relation [69]:

$$(\alpha h\nu) = Ao(h\nu - E_g)^{1/2},$$

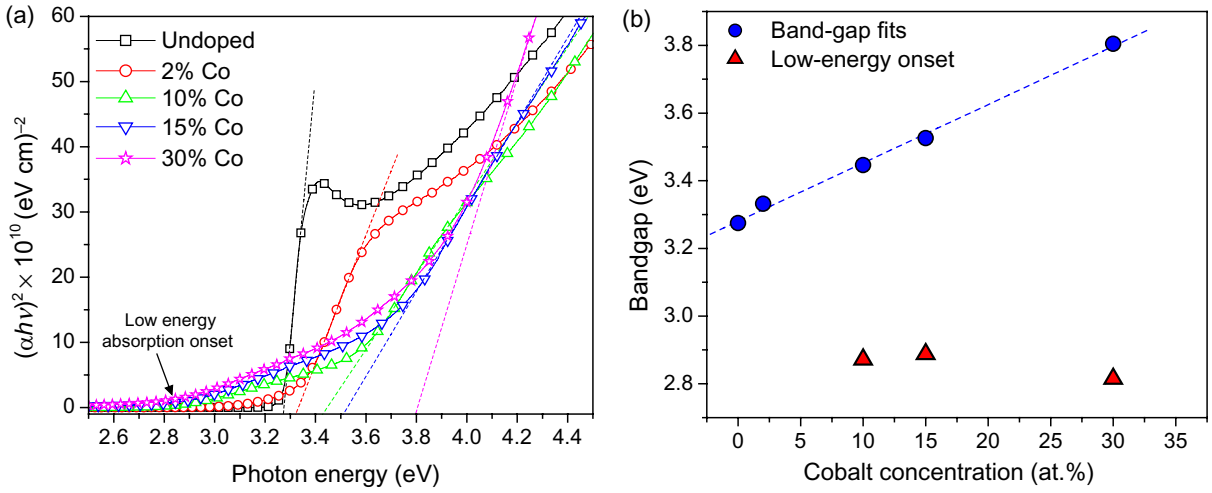

Figure 12. Optical bandgap plots for Co-doped ZnO films deposited in vacuum at 400 °C. (a) Plots of $(\alpha h\nu)^2$ versus $h\nu$. Straight line fits through the linear regions of the plot are extrapolated to $h\nu = 0$ to find the bandgap. (b) Plot of the bandgap values as a function of nominal cobalt concentration. Filled circles are the bandgap and hollow triangles represent the onset of absorption at low energy.

where $h\nu$ is the photon energy, E_g is the bandgap, and A_o is a parameter associated with the transition probability. α was calculated from the absorbance data using $\alpha = (2.3 \times A/t)$, where A is the absorbance and t is the film thickness. The bandgap was calculated by plotting $(\alpha h\nu)^2$ versus $h\nu$ and extrapolating the linear portion of the plot to $(\alpha h\nu)^2 = 0$. The plots are given in figure 12(a). At low cobalt doping—the undoped film and the film doped with 2% Co—the absorption edge is well defined and can be fit reliably. The exciton peak is clearly visible in the undoped film indicating good quality ZnO. However, as the cobalt doping is increased, band tailing becomes evident in the data with the onset of absorption at lower energy, and the doping smears out the linear region making a more rounded shape. The character of the bandgap may be becoming more indirect with added cobalt. Linear fits to both the high- and low-energy regions are shown in figure 12(b) as a function of cobalt concentration. The high-energy slopes give a bandgap energy that linearly increases (blue-shifts) with cobalt concentration. The low-energy slopes represent the onset of absorption and give an energy that roughly remains constant around 2.8–2.9 eV.

Some reports in the literature observe a red-shift in the bandgap energy as the cobalt concentration is increased [70]–[73]. The red-shift is typically attributed to the sp–d exchange between the ZnO band electrons and localized d-electrons associated with the doped Co^{+2} cations. The interaction leads to corrections in the energy bands; the conduction band is lowered and the valence band is raised causing the bandgap to shrink [74]. On the other hand, other papers have reported a blue-shift in the bandgap of ZnO with cobalt doping. Peng *et al* [75] reported a blue-shift in the bandgap of the material and a red-shift of the band tails, which is similar to our observations. Ozerov *et al* [64] also reported a blue-shift in the bandgap in nanocrystalline films. Yoo *et al* [76] observed a blue-shift in Al- and Co-codoped ZnO films which was attributed to the Burnstein–Moss effect from an increase in the carrier concentration.

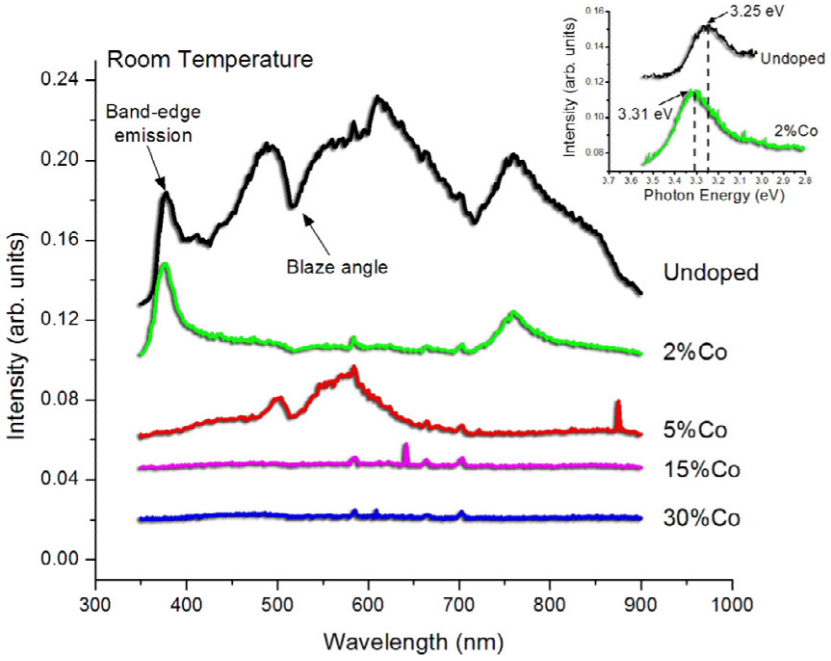

Figure 13. Room temperature PL results for Co-doped ZnO films deposited in vacuum at 400 °C. The dip in the PL spectra at ∼517 nm is an artifact from the diffraction grading blaze angle. The PL intensity disappears with higher cobalt doping. The inset shows higher resolution scans around the band-edge peak for the undoped and 2% Co samples. The values correspond well with the absorption data.

The absorption at low energy in higher doped films may indicate the formation of cobalt derived states near the band edge. Band tails can arise from perturbations in the band structure caused by impurities and disorder. States introduced by impurities overlap at high concentrations and evolve into an impurity band. As seen in figure 12(a), the tails' intensity rises with increased cobalt. Therefore, the tails are most likely related to the increase of impurity states. Kittilstved *et al* saw a large MCD peak at ∼25 000 cm^{-1} (3.10 eV), which they assigned as a valence band-to-metal CT transition in Co-doped ZnO [25]. The level was approximately 2600 cm^{-1} (0.322 eV) below the conduction band. The onset of absorption in figure 12 starts around 2.9 eV. Therefore, the low-energy absorption onset is likely an electron transition from the valence band to cobalt-derived impurity states.

Photoluminescence (PL) was performed on the series of films grown at 400 °C in vacuum. The PL was used primarily to verify the bandgap shift found in the optical absorption data. Figure 13 shows the PL spectra taken at room temperature. For the undoped and 5% Co film, a broad luminescence band is visible across the spectrum. Broad green-yellow bands are typically attributed to defects in ZnO, including oxygen vacancies [77]. The films are grown in low-oxygen pressures and are non-stoichiometric which could give rise to the broad defect bands. A more detailed study of the low temperature PL properties would have to be done to say more about the bands. The dip in the intensity at ∼517 nm is an artifact due to the blaze angle of the diffraction grating and not from the film properties. The band edge is visible in the undoped and 2% Co-doped films, but is quenched with higher cobalt doping. This is consistent with the

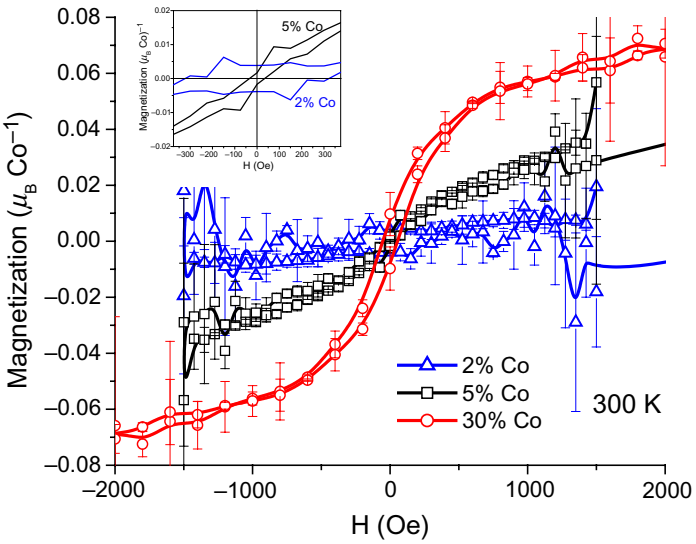

Figure 14. Room temperature SQUID magnetization curves for films deposited at 400 °C in vacuum with 2, 5 and 30% Co.

change in shape of the Tauc plots presented in figure 12 and a change in the character of band-to-band excitation. Higher resolution scans around the band-edge emissions of the undoped and 2% Co samples are shown in the inset of figure 13. The band edge is blue-shifted from 3.25 to 3.31 eV in the 2% Co sample, which is consistent with the bandgaps determined from optical absorption.

3.4. Magnetic characterization

The volume magnetization of the films was measured using a Quantum Design SQUID magnetometer. Before measuring, the backs and sides of the samples were etched in nitric acid (50% nitric/50% deionized water) to remove excess silver paint and contaminants that could contribute a spurious magnetic signal measured by the SQUID. Each film surface was first coated in photoresist and baked for 20 min at 50 °C to help protect the film during etching, and then floated on top of the nitric acid for 3 min. The photoresist was removed by rinsing in acetone. The SQUID magnetization data are normalized by the number of Bohr magnetons (μ_B) per Co atom. To convert the raw magnetization data from emu units to μ_B/Co, the cobalt atoms are assumed to occupy Zn sites and a cation density of 4.18×10^{22} cm^{-3} is used for the conversion. The data are normalized using the cobalt concentrations from the EDS data given in figure 1.

Magnetization data taken at 300 K for a series of films grown at 400 °C under vacuum with different amounts of cobalt are displayed in figure 14. Films grown in higher oxygen pressures (up to 20 mTorr) show very little, if any, magnetization. Films doped with 2 and 5% cobalt show smaller magnetization than the more heavily alloyed film. The hysteresis curves for the 2 and 5% samples are not well developed. A closer look reveals that the curves have a broadening at low field, which appears to be an additional component to the curve (inset of figure 14). This may represent a small ferromagnetic component superimposed on an overall paramagnetic state. This is consistent with other reports that the Co sublattice is paramagnetic while an additional ferromagnetic component is present, presumably from defects in the anion

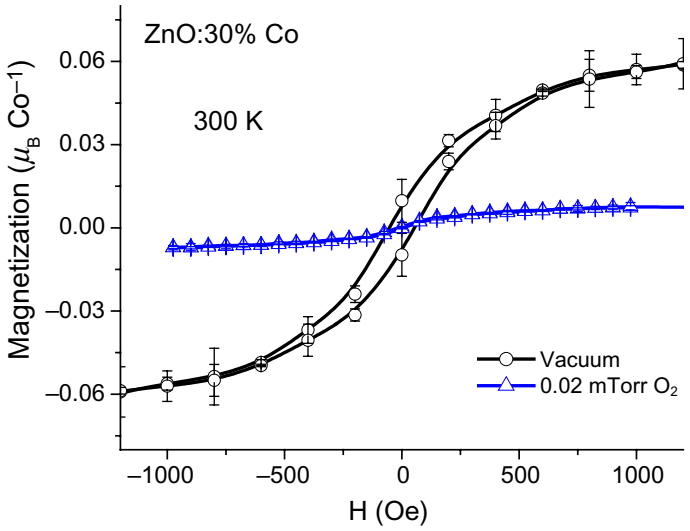

Figure 15. Room temperature magnetic hysteresis curves for 30% Co-doped films deposited at 400 C under vacuum and in 0.02m Torr O_2.

sublattice [36]. However, this behavior is not apparent in the 30% Co-doped film. The 30% Co film shows ferromagnetism up to 300 K with a clear hysteretic shape. The sample has a room temperature magnetization approaching $0.08u_B$/Co at an applied field of 3 T. Additionally, a film doped with 30% Co that showed some metallic cobalt segregation (a film deposited at low-base pressure) was measured and displayed a room temperature saturation of around $0.22\mu_B$/Co (not shown).

At higher pressures the FM moment decreases considerably. Figure 15 shows the comparison between room temperature SQUID measurements for 30% Co-doped films prepared in vacuum and in 0.02 mTorr O_2. Neither of these films shows metallic cobalt precipitation by XRD. There is a 10-fold reduction in the saturation magnetization ($M_s \sim 0.009\mu_B$/Co) and the hysteresis loop closes to a coercivity of 10 Oe. The decrease in ferromagnetism in the presence of molecular oxygen is evidence that the intrinsic growth defects in ZnO play a significant role in mediating the observed magnetic properties. It is worth noting that the room temperature resistivity increases from 0.566 ohm-cm when grown in vacuum to 5.579 ohm-cm when grown in 0.02 mTorr O_2 indicating a change in the defect concentration.

Theoretical modeling shows that Co^{+2}–oxygen vacancy (Co–Ov) pairs are capable of producing a long-range ferromagnetic ground state in ZnO [40]. A concentration of about 6% Co–Ov pairs is estimated to place ZnO in the ferromagnetic state and produce exchange couplings large enough to produce the anomalous Hall effect in transport measurements [40]. We have observed the presence of the anomalous Hall effect at room temperature in selected films, including films doped with 15 and 30% cobalt, which will be the focus of a future publication.

Another factor to consider is the low magnetic saturation in these films. The high-spin moment ($3d^7$) of Co^{+2} is $3\mu_B$, while that of metallic cobalt is $1.7\mu_B$. The saturation magnetization of the 30% Co-doped film is rather small at $0.08\mu_B\,Co^{-1}$. This small value, however, is in good agreement with reports on Co-doped ZnO that has been modified by vacuum annealing [37] or by Zn vapor anneals [38]. Also, the increased magnetization with cobalt concentration is in agreement with some results [78] and in contrast with others that

show a decreasing magnetization with increasing cobalt concentration [30]. The exchange coupling between Co–Co nearest-neighbors in ZnO is believed to be antiferromagnetic [79], thus large concentrations of Co–Co pairs should reduce the overall moment. So there are likely competing mechanisms between regions of Co–defect pair ferromagnetism, Co–Co nearest-neighbor antiferromagnetic exchange, and isolated cobalt atoms that act paramagnetically. At large concentrations, there may be enough Co–defect pairs to produce FM, but this will be compensated by Co pairs that are antiferromagnetically aligned, which will reduce the overall moment per cobalt atom. The small observed moment in these films is likely a result of the competing mechanisms. The larger magnetization from depositing in an oxygen-deficient environment suggests oxygen vacancies are responsible, but the unintentional incorporation of hydrogen during growth under higher residual base pressures is also a possibility. It has been suggested that hydrogen could play a role in mediating ferromagnetism in transition metal doped ZnO [80]. It is known that hydrogen easily diffuses into and out of ZnO at moderate temperatures [81], and recent experiments suggest some correlation between magnetization and hydrogen content in transition metal doped ZnO [82].

In summary, low growth pressure conditions are needed to create the oxygen vacancies that seem to be the necessary ingredient for ferromagnetic behavior. However, enough oxygen must be present during growth to stabilize cobalt in higher oxidation states and suppress metallic cobalt precipitation. We also find that if the temperature is too high ($T \geqslant 500\,^{\circ}\mathrm{C}$) the cobalt atoms do not occupy Zn sites, but tend to form the more thermodynamically stable CoO phase. Thus growth conditions must be tuned appropriately to control the structure–property relationship necessary for ferromagnetism. Post-growth annealing treatments to create the required defects may provide better control of the magnetic properties, such as that demonstrated in the digital 'on/off' control of ferromagnetism [38].

4. Conclusion

The structure and magnetic properties of Co-doped ZnO films were studied in respect to cobalt concentration and growth conditions. Films with a few per cent of cobalt show a combination of ferromagnetic and paramagnetic behavior at room temperature with a small moment per cobalt atom. Films doped with 30% Co deposited in vacuum show ferromagnetism at room temperature with a saturation magnetization of $0.08\mu_{\mathrm{B}}$/Co and a coercivity of 60 Oe. However, depositing in a small amount of molecular oxygen considerably quenches the ferromagnetism in these films. Oxygen vacancy defects created during vacuum growth are the likely ingredient necessary for the observed ferromagnetism. The small moment per cobalt atom is probably from competing effects between FM Co–defect pairs, AFM Co–Co nearest-neighbors, and paramagnetic isolated Co atoms.

Microstructural characterization focused on films doped with 30% Co as these showed interesting magnetic and structural properties. Optical absorption and XPS showed a large amount of Co^{+2} within the ZnO lattice. Bright-field TEM and electron diffraction seem to indicate a homogeneous solid solution of cobalt in the ZnO. However, areas of bright contrast are evident in dark-field imaging which could be associated with precipitation. XPS also indicates some metallic cobalt in the films, but could be associated with a surface of sputter reduced cobalt atoms.

Difficulties in determining the atomic-level microstructure are likely one source of the discrepancies between results from different research groups. Especially if the magnetic

properties rely on an intricate combination of transition metal dopants and material defects, such as oxygen vacancies which are difficult to characterize. Our studies show that both the structural and magnetic properties can depend sensitively on film growth parameters. Thus, a complete understanding of these systems will require further studies of the structure–property relationships.

Acknowledgments

We thank the staff and facilities of the Major Analytical Instrumentation Center, Department of Materials Science and Engineering, University of Florida; especially Dr Valentin Craciun, Kerry Siebein and Eric Lambers. This work was partially supported by NSF (DMR 0704240). The ORNL research is sponsored by the Division of Materials Science, the US Department of Energy, under contract with the UT-Battelle, LLC.

References

[1] Wolf S A, Awschalom D D, Buhrman R A, Daughton J M, Von Molnar S, Roukes M L, Chtchelkanova A Y and Treger D M 2001 Spintronics: a spin-based electronics vision for the future *Science* **294** 1488–95

[2] Pearton S J, Norton D P, Frazier R, Han S Y, Abernathy C R and Zavada J M 2005 Spintronics device concepts *IEEE Proc. Circuits Devices Syst.* **152** 312–22

[3] Ohno H, Chiba D, Matsukura F, Omlya T, Abe E, Dietl T, Ohno Y and Ohtani K 2000 Electric-field control of ferromagnetism *Nature* **408** 944–46

[4] Schallenberg T and Munekata H 2006 Preparation of ferromagnetic (In,Mn)As with a high Curie temperature of 90 K *Appl. Phys. Lett.* **89** 042507

[5] Nazmul A M, Sugahara S and Tanaka M 2003 Ferromagnetism and high Curie temperature in semiconductor heterostructures with Mn delta-doped GaAs and p-type selective doping *Phys. Rev.* B **67** 241308

[6] Pearton S J, Abernathy C R, Norton D P, Hebard A F, Park Y D, Boatner L A and Budai J D 2003 Advances in wide bandgap materials for semiconductor spintronics *Mater. Sci. Eng.* R **40** 137

[7] Chambers S A 2006 Ferromagnetism in doped thin-film oxide and nitride semiconductors and dielectrics *Surf. Sci. Rep.* **61** 345–81

[8] Pearton S J, Norton D P, Ip K, Heo Y W and Steiner T 2003 Recent progress in processing and properties of ZnO *Superlatt. Microstruct.* **34** 3–32

[9] Jeong B S, Heo Y W, Norton D P, Kelly J G, Rairigh R, Hebard A F, Budai J D and Park Y D 2004 Spatial distribution and electronic state of Co in epitaxial anatase $Co_xTi_{1-x}O_2$ thin films grown by reactive sputtering *Appl. Phys. Lett.* **84** 2608–10

[10] Ivill M, Overberg M E, Abernathy C R, Norton D P, Hebard A F, Theodoropoulou N and Budai J D 2003 Properties of Mn-doped Cu_2O semiconducting thin films grown by pulsed-laser deposition *Solid-State Electron.* **47** 2215–20

[11] Dietl T, Ohno H, Matsukura F, Cibert J and Ferrand D 2000 Zener model description of ferromagnetism in zinc-blende magnetic semiconductors *Science* **287** 1019–22

[12] Ip K *et al* 2003 Ferromagnetism in Mn- and Co-implanted ZnO nanorods *J. Vac. Sci. Technol.* B **21** 1476–81

[13] Pearton S J *et al* 2004 Wide bandgap GaN-based semiconductors for spintronics *J. Phys: Condens. Matter* **16** R209–45

[14] Pearton S J *et al* 2003 Effects of defects and doping on wide band gap ferromagnetic semiconductors *Physica* B **340–342** 39–47

[15] Pearton S J, Norton D P, Heo Y W, Tien L C, Ivill M P, Li Y, Kang B S, Ren F, Kelly J and Hebard A F 2006 ZnO spintronics and nanowire devices *J. Electron. Mater.* **35** 862–8

[16] Theodoropoulou N A *et al* 2003 Ferromagnetism in Co- and Mn-doped ZnO *Solid-State Electron.* **47** 2231–35

[17] Zukova A, Teiserskis A, Kazlauskiene V, Gun'ko Y K and Van Dijken S 2007 Structural and magnetic properties of Co-doped ZnO films grown by pulse-injection MOCVD *J. Magn. Magn. Mater.* **316** E203–6
[18] Gacic M, Jakob G, Herbort C, Adrian H, Tietze T, Bruck S and Goering E 2007 Magnetism of Co-doped ZnO thin films *Phys. Rev.* B **75** 205206
[19] Bhatti K P, Chaudhary S, Pandya D K and Kashyap S C 2007 Intrinsic and extrinsic origin of room temperature ferromagnetism in ZnO:Co (5 at.%) *J. Appl. Phys.* **101** 103919
[20] Schmidt H, Diaconu M, Hochmuth H, Benndorf G, von Wenckstern H, Biehne G, Lorenz M and Grundmann M 2007 Electrical and optical spectroscopy on ZnO:Co thin films *Appl. Phys. A: Mater.* **88** 157–60
[21] Shi T, Zhu S, Sun Z, Wei S and Liu W 2007 Structures and magnetic properties of wurtzite $Zn_{1-x}Co_xO$ dilute magnetic semiconductor nanocomposites *Appl. Phys. Lett.* **90** 102108
[22] Bhatti K P, Chaudhary S, Pandya D K and Kashyap S C 2007 High temperature investigation of the magnetization behavior in cobalt substituted ZnO *J. Appl. Phys.* **101** 033902
[23] Quesada A, Garcia M A, Andres M, Hernando A, Fernandez J F, Caballero A C, Martin-Gonzalez M S and Briones F 2006 Ferromagnetism in bulk Co-Zn-O *J. Appl. Phys.* **100** 113909
[24] Coey J M D, Venkatesan M and Fitzgerald C B 2005 Donor impurity band exchange in dilute ferromagnetic oxides *Nat. Mater.* **4** 173–9
[25] Kittilstved K R, Liu W K and Gamelin D R 2006 Electronic structure origins of polarity-dependent high-TC ferromagnetism in oxide-diluted magnetic semiconductors *Nat. Mater.* **5** 291–7
[26] Ivill M, Pearton S J, Norton D P, Kelly J and Hebard A F 2005 Magnetization dependence on electron density in epitaxial ZnO thin films codoped with Mn and Sn *J. Appl. Phys.* **97** 053904
[27] Ivill M, Pearton S J, Heo Y W, Kelly J, Hebard A F and Norton D P 2007 Magnetization dependence on carrier doping in epitaxial ZnO thin films co-doped with Mn and P *J. Appl. Phys.* **101** 123909
[28] Ueda K, Tabata H and Kawai T 2001 Magnetic and electric properties of transition-metal-doped ZnO films *Appl. Phys. Lett.* **79** 988
[29] Ramachandran S, Tiwari A and Narayan J 2004 $Zn_{0.9}Co_{0.1}O$-based diluted magnetic semiconducting thin films *Appl. Phys. Lett.* **84** 5255–57
[30] Fitzgerald C B, Venkatesan M, Lunney J G, Dorneles L S and Coey J M D 2005 Cobalt-doped ZnO—a room temperature dilute magnetic semiconductor *Appl. Surf. Sci.* **247** 493–6
[31] Dinia A, Schmerber Meny C, Pierron-Bohnes V and Beaurepaire E 2005 Room-temperature ferromagnetism in $Zn_{1-x}Co_xO$ magnetic semiconductors prepared by sputtering *J. Appl. Phys.* **97** 123908
[32] Lawes G, Risbud A S, Ramirez A P and Seshadri R 2005 Absence of ferromagnetism in Co and Mn substituted polycrystalline ZnO *Phys. Rev.* B **71** 045201
[33] Jin Z *et al* 2001 *Appl. Phys. Lett.* **78** 3824
[34] Park J H, Kim M G, Jang H M, Ryu S and Kim Y M 2004 Co-metal clustering as the origin of ferromagnetism in Co-doped ZnO thin films *Appl. Phys. Lett.* **84** 1338
[35] Kim J H, Kim H, Kim D, Ihm Y E and Choo W K 2002 Magnetic properties of epitaxially grown semiconducting $Zn_{1-x}Co_xO$ thin films by pulsed laser deposition *J. Appl. Phys.* **92** 6066–71
[36] Barla A *et al* 2007 Paramagnetism of the Co sublattice in ferromagnetic $Zn_{1-x}Co_xO$ films *Phys. Rev.* B **76** 125201
[37] Tuan A C *et al* 2004 Epitaxial growth and properties of cobalt-doped ZnO on alpha-Al_2O_3 single-crystal substrates *Phys. Rev.* B **70** 054424
[38] Schwartz D A and Gamelin D R 2004 Reversible 300 K ferromagnetic ordering in a diluted magnetic semiconductor *Adv. Mater.* **16** 2115–19
[39] Khare N, Kappers M J, Wei M, Blamire M G and MacManus-Driscoll J L 2006 Defect-induced ferromagnetism in Co-doped ZnO *Adv. Mater.* **18** 1449
[40] Pemmaraju C D, Hanafin R, Archer T, Braun H B and Sanvito S 2008 Impurity-ion pair induced high-temperature ferromagnetism in Co-doped ZnO *Preprint* 0801.4945v1 [cond-mat.mtrl-sci]
[41] Coey J M D, Venkatesan M, Stamenov P, Fitzgerald C B and Dorneles L S 2005 Magnetism in hafnium dioxide *Phys. Rev.* B **72** 024450

[42] Norton D P 2004 Synthesis and properties of epitaxial electronic oxide thin-film materials *Mater. Sci. Eng.* R **43** 139–247
[43] Dorneles L S, O'Mahony D, Fitzgerald C B, McGee F, Venkatesan M, Stanca I, Lunney J G and Coey J M D 2005 Structural and compositional analysis of transition-metal-doped ZnO and GaN PLD thin films *Appl. Surf. Sci.* **248** 406–10
[44] Xu Q, Hartmann L, Schmidt H, Hochmuth H, Lorenz M, Schmidt-Grund R, Spemann D, Rahm A and Grundmann M 2006 Magnetoresistance in pulsed laser deposited 3d transition metal doped ZnO films *Thin Solid Films* **515** 2549–54
[45] Zhou H *et al* 2007 Raman studies of ZnO:Co thin films *Phys. Status Solidi* a **204** 112–7
[46] Zhang H and Chen X 2005 Controlled synthesis and anomalous magnetic properties of relatively monodisperse CoO nanocrystals *Nanotechnology* **16** 2288–94
[47] Ichiyanagi Y, Kimishima Y and Yamada S 2004 Magnetic study on Co_3O_4 nanoparticles *J. Magn. Magn. Mater.* **272–276** E1245–46
[48] Kim H J, Song I C, Sim J H, Kim H, Kim D, Ihm Y E and Choo W K 2004 Growth and characterization of spinel-type magnetic semiconductor $ZnCo_2O_4$ by reactive magnetron sputtering *Phys. Status Solidi* b **241** 1553–6
[49] Dinia A, Ayoub J P, Schmerber G, Beaurepaire E, Muller D and Grob J J 2004 Effect of ion irradiation on the structural and the magnetic properties of $Zn_{0.75}Co_{0.25}$ magnetic semiconductors *Phys. Lett.* A **333** 152–6
[50] Sutta P 2000 Lattice stress gradients in thin films deposited by reactive sputtering *ASDAM 2000 Int. EuroConf. on Advanced Semiconductor Devices and Microsystems, Conf. Proc., 3rd (Smolenice Castle, Slovakia)* p 323
[51] Norton D P *et al* 2003 Ferromagnetism in cobalt-implanted ZnO *Appl. Phys. Lett.* **83** 5488–90
[52] Barin I 1995 *Thermochemical Data of Pure Substances* (New York: VCH)
[53] Wagner C D, Naumkin A V, Kraut-Vass A, Allison J W, Powell C J and Rumble J R Jr 2003 NIST X-ray Photoelectron Spectroscopy Database, Version 3.4 (Web version: http://srdata.nist.gov/xps/)
[54] Wagner C D, Davis L E, Moulder J F and Mullenberg G E 1978 *Handbook of X-ray Photoelectron Spectroscopy* (Minnesota: Perkin-Elmer Corporation)
[55] Choudhury T, Saied S O, Sullivan J L and Abbot A M 1989 Reduction of oxides of iron, cobalt, titanium and niobium by low-energy ion bombardment *J. Phys. D: Appl. Phys.* **22** 1185–95
[56] Powell R A, Spicer W E and McMenamin J C 1972 Photoemission studies of wurtzite zinc oxide *Phys. Rev.* B **6** 3056
[57] Jin Z, Murakami M, Fukumura T, Matsumoto Y, Ohtomo A, Kawasaki M and Koinuma H 2000 Combinatorial laser MBE synthesis of 3d ion doped epitaxial ZnO thin films *J. Cryst. Growth* **214–215** 55
[58] Park J H, Kim M G, Jang H M, Ryu S and Kim Y M 2004 Co-metal clustering as the origin of ferromagnetism in Co-doped ZnO thin films *Appl. Phys. Lett.* **84** 1338
[59] Kittilstved K R, Schwartz D A, Tuan A C, Heald S M, Chambers S A and Gamelin D R 2006 Direct kinetic correlation of carriers and ferromagnetism in Co^{+2}: ZnO *Phys. Rev. Lett.* **97** 037203
[60] Lee H J, Jeong S Y, Cho C R and Park C H 2002 Study of diluted magnetic semiconductor: Co-doped ZnO *Appl. Phys. Lett.* **81** 4020
[61] Duan L B, Chu W G, Yu J, Wang Y C, Zhang L N, Liu G Y, Liang J K and Rao G H 2008 Structural and magnetic properties of $Zn_{1-x}Co_xO$ ($0 < x \leqslant 0.30$) nanoparticles *J. Magn. Magn. Mater.* **320** 1573–81
[62] Liu Q, Yuan C L, Gan C L and Han G C 2007 *J. Appl. Phys.* **101** 073902
[63] Lee S S, Kim G, Wi S C, Kang J S, Han S W, Lee Y K, An K S, Kwon S J, Jung M H and Shin H J 2006 Investigation of the phase separations and the local electronic structures of $Zn_{1-x}T_xO$ (T = Mn, Fe, Co) magnetic semiconductors using synchrotron radiation *J. Appl. Phys.* **99** 08M103
[64] Ozerov I, Chabre F and Marine W 2005 Incorporation of cobalt into ZnO nanoclusters *Mater. Sci. Eng.* C **25** 614
[65] Hsu H S, Huang J C A, Huang Y H, Liao Y F, Lin M Z, Lee C H, Lee J F, Chen S F, Lai L Y and Liu C P 2006 Evidence of oxygen vacancy enhanced room-temperature ferromagnetism in Co-doped ZnO *Appl. Phys. Lett.* **88** 242507

[66] Song C, Zeng F, Geng K W, Wang X B, Shen Y X and Pan F 2007 The magnetic properties of Co-doped ZnO diluted magnetic insulator films prepared by direct current reactive magnetron co-sputtering *J. Magn. Magn. Mater.* **309** 25–30
[67] Samanta K, Bhattacharya P and Katiyar R S 2005 Optical properties of $Zn_{1-x}Co_xO$ thin films grown on Al_2O_3 (0001) substrates *Appl. Phys. Lett.* **87** 101903
[68] Koidl P 1977 Optical absorption of Co^{2+} in ZnO *Phys. Rev.* B **15** 2493–99
[69] Simmons J H and Potter K S 2000 *Optical Materials* (New York: Academic) p 391
[70] Kim K J and Park Y R 2002 Spectroscopic ellipsometry study of optical transitions in $Zn_{1-x}Co_xO$ alloys *Appl. Phys. Lett.* **81** 1420
[71] Bouloudenine M, Viart N, Colis S and Dinia A 2004 Bulk $Zn_{1-x}Co_xO$ magnetic semiconductors prepared by hydrothermal technique *Chem. Phys. Lett.* **397** 73–6
[72] Bhat S V and Deepak F L 2005 Tuning the bandgap of ZnO by substitution with Mn^{2+}, Co^{2+} and Ni^{2+} *Solid State Commun.* **135** 345–47
[73] Liu X, Shi E, Chen Z, Zhang H, Song L, Wang H and Yao S 2006 Structural, optical and magnetic properties of Co-doped ZnO films *J. Cryst. Growth* **296** 135–40
[74] Lee Y R, Ramdas A K and Aggarwal R L 1988 Energy gap, excitonic, and internal Mn^{2+} optical transition in Mn-based II–VI diluted magnetic emiconductors *Phys. Rev.* B **38** 10600–10
[75] Peng Y Z, Liew T, Song W D, An C W, Teo K L and Chong T C 2005 Structural and optical properties of Co-doped ZnO thin films *J. Supercond.* **18** 97–103
[76] Yoo Y, Fukumura T, Jin Z, Hasegawa K, Kawasaki M, Ahmet P, Chikyow T and Koinuma H 2001 ZnO–CoO solid solution thin films *J. Appl. Phys.* **90** 4246
[77] Ozgur U, Alivov Y I, Liu C, Teke A, Reshchikov M A, Dogan S, Avrutin V, Cho S and Morkoc H 2005 A comprehensive review of ZnO materials and devices *J. Appl. Phys.* **98** 041301
[78] Lim S W, Hwang D K and Myoung J M 2003 Observation of optical properties related to room-temperature ferromagnetism in co-sputtered $Zn_{1-x}Co_xO$ thin films *Solid State Commun.* **125** 231
[79] Chanier T, Sargolzaei M, Opahle I, Hayn R and Koepernik K 2006 LSDA + U versus LSDA: towards a better description of the magnetic nearest-neighbor exchange coupling in Co- and Mn-doped ZnO *Phys. Rev.* B **73** 134418
[80] Park C H and Chadi D J 2005 Hydrogen-mediated spin–spin interaction in ZnCoO *Phys. Rev. Lett.* **94** 127204
[81] Ip K, Overberg M E, Heo Y W, Norton D P, Pearton S J, Stutz C E, Luo B, Ren F, Look D C and Zavada J M 2003 Hydrogen incorporation and diffusivity in plasma-exposed bulk ZnO *Appl. Phys. Lett.* **82** 385–7
[82] Jayakumar O D, Gopalakrishnan I K, Shashikala K, Kulshreshtha S K and Sudakar C 2006 Magnetic properties of hydrogenated Li and Co doped ZnO nanoparticles *Appl. Phys. Lett.* **89** 202507